Classification: Physical and Biological Sciences

Munc13-1 MUN domain and Munc18-1 cooperatively chaperone SNARE assembly through a tetrameric complex

Tong Shu[a,b,c], Huaizhou Jin[a], James E. Rothman[a,1], and Yongli Zhang[a,1]

[a]Department of Cell Biology, Yale University School of Medicine, New Haven, CT 06520
[b]Integrated Graduate Program in Physical and Engineering Biology,
[c]Department of Physics, Yale University, New Haven, CT 06511.

[1]To whom correspondence may be addressed: yongli.zhang@yale.edu or james.rothman@yale.edu

Abstract

Munc13-1 is a large multi-functional protein essential for synaptic vesicle fusion and neurotransmitter release. Its dysfunction has been linked to many neurological disorders. Evidence suggests that the MUN domain of Munc13-1 collaborates with Munc18-1 to initiate SNARE assembly, thereby priming vesicles for fast calcium-triggered vesicle fusion. The underlying molecular mechanism, however, is poorly understood. Recently, it was found that Munc18-1 catalyzes neuronal SNARE assembly through an obligate template complex intermediate containing Munc18-1 and two SNARE proteins – syntaxin 1 and VAMP2. Here, using single-molecule force spectroscopy, we discovered that the MUN domain of Munc13-1 stabilizes the template complex by approximately 2.1 k_BT. The MUN-bound template complex enhances SNAP-25 binding to the templated SNAREs and subsequent full SNARE assembly. Mutational studies suggest that the MUN-bound template complex is functionally important for SNARE assembly and neurotransmitter release. Taken together, our observations provide a potential molecular mechanism by which Munc13-1 and Munc18-1 cooperatively chaperone SNARE folding and assembly, thereby regulating synaptic vesicle fusion.

Keywords

SNARE assembly, Munc13-1, Munc18-1, template complex, optical tweezers

Significance

Neurons in the brain communicate with each other by release of neurotransmitters. Neurotransmitter release is mediated by three membrane-anchored SNARE proteins and various regulatory proteins, including Munc13-1 and Munc18-1. SNAREs couple their folding and assembly to membrane fusion in a regulatory protein-dependent manner. The physiological pathway of the

regulated SNARE assembly, however, is unclear. We found that the MUN domain of Munc13-1, Munc18-1, and two SNAREs – syntaxin 1 and VAMP2 associate into a weak tetrameric complex. The third SNARE protein SNAP-25B rapidly binds the two SNAREs in the complex to form a ternary SNARE complex likely with a displacement of the regulatory proteins. Therefore, Munc13-1 and Munc18-1 cooperatively chaperone SNARE assembly, a process required for neurotransmitter release.

\body

Neurotransmission relies on synaptic vesicle fusion and the corresponding release of neurotransmitters into the synaptic junction (1, 2). Various proteins mediate and control the fusion process with high precision (3, 4). Key proteins include three membrane-anchored SNARE proteins – syntaxin 1 and SNAP-25 on the plasma membrane and VAMP2 (or synaptobrevin 2) on the vesicle membrane (5, 6) and at least five regulatory proteins – Munc13-1, Munc18-1, synaptotagmin, complexin, and NSF (4, 7, 8). SNARE proteins consist of characteristic SNARE motifs of ~ 60 amino acids, which are intrinsically disordered in solution. Coupled folding and assembly of the four SNARE motifs in the three SNAREs into a four-helix bundle draw their associated membranes into proximity, inducing membrane fusion (9-11). Synaptotagmin and complexin suspend the assembly of the membrane-bridging trans-SNARE complex midway but promote its full assembly and membrane fusion when triggered by calcium upon the arrival of an action potential (3, 7, 12-14). After fusion, NSF and its adaptor protein SNAP disassemble the fully assembled cis-SNARE complex in an ATP-dependent manner for next round of SNARE assembly (15, 16). Despite decades of research, it remains unclear how SNAREs and regulatory proteins collaborate to drive membrane fusion.

Both Munc13-1 and Munc18-1 initiate SNARE assembly and help prime synaptic vesicles for subsequent Ca^{2+}-triggered fusion (17-21). Evolutionarily unrelated, Munc13-1 and Munc18-1 were first identified as *m*ammalian homologues of Unc13 and Unc18, respectively, C. elegans mutations that cause *unc*oordinated motion (22). Munc13-1 is a large multi-functional rod-like protein containing N-terminal C_2A, C_1, and C_2B domains, a central MUN domain, and a C-terminal C_2C domain (Fig. 1A) (23-25). Munc13-1 has been shown to promote membrane fusion by two means: it tethers synaptic vesicles to the plasma membrane through its N- and C-terminal C_2 and C_1 domains (23, 26-29) and directly enhances SNARE assembly through the MUN domain (19, 25, 30-32). The latter activity has been recapitulated using the isolated MUN domain in vitro and requires its weak binding to both syntaxin 1 and VAMP2 with affinities of 40-110 μM (19, 24, 30-32). Recently, Munc13-1 was shown to cooperate with Munc18-1 to promote the accuracy of SNARE assembly (19). Munc18-1 tightly associates with syntaxin 1 in a closed conformation that inhibits syntaxin association with other SNAREs (33-36). However, the closed syntaxin likely serves as a starting syntaxin conformation in vivo and must be opened for SNARE assembly (18, 25). Interestingly, with mutations that destabilize the closed conformation of syntaxin, Munc18-1 binds both syntaxin 1 and VAMP2 to form a ternary template complex (37, 38). In the complex, the N-terminal regions of the SNARE motifs of both SNAREs are aligned in helical conformations on the surface of Munc18-1, while the C-terminal regions are kept separated. The templated SNAREs nucleate SNAP-25B association and proper SNARE assembly. Mutation experiments suggest that the stability of the template complex correlates with the rate of SNARE assembly or membrane fusion. Consistent with these observations, it has been hypothesized that Munc13-1 stabilizes the template complex (37). However, an experimental test of this hypothesis has been lacking.

We investigated SNARE assembly in the presence of both the MUN domain of Munc13-1 and Munc18-1 using optical tweezers. We found that the MUN domain indeed stabilizes the template complex and significantly promotes SNAP-25 binding and SNARE assembly. Thus, Munc13-1 and Munc18-1 cooperatively chaperone SNARE assembly.

Results

MUN domain stabilizes the template complex. We modified our previous experimental setup for pulling a single SNARE complex (Fig. 1B) (37). As before, syntaxin 1A and VAMP2 were crosslinked at their N-termini (between syntaxin R198C and VAMP2 N29C) and pulled from their C-termini via two optical trapped beads. Because the MUN domain is ~16 nm long (23), we introduced a second DNA handle of ~500 bp to isolate any MUN-SNARE complex from bead surfaces and thereby minimize potential nonspecific interactions. The MUN domain and Munc18-1, either alone or together, were added into the solution. To facilitate protein preparation, we used the recombinant MUN domain as in previous experiments (19, 25, 30, 31). The folding and unfolding transitions of the SNARE proteins in response to the pulling force and binding of the regulatory proteins were measured by the extension change of the protein-DNA tether with sub-nanometer and sub-millisecond resolution (39-41).

We first pulled a single SNARE complex in the absence of any regulatory protein. The resultant force-extension curve (FEC, Fig. 1C, grey curve in FEC#1) indicated that a single SNARE complex unfolded in a stepwise manner (SI Appendix, Fig. S1): reversible C-terminal domain (CTD) transition (Fig. 1B, oval region), irreversible N-terminal domain (NTD) unfolding (gray arrow), and irreversible t-SNARE unfolding and the accompanying SNAP-25B dissociation (green arrow) (11). Relaxing the remaining SNARE proteins did not reveal any refolding events,

suggesting minimum interactions between syntaxin 1 and VAMP2. However, the addition of 1 μM Munc18-1 induced two reversible transitions seen in the first relaxation curve (#2, black curve) and subsequent pulling and relaxation curves (#3, cyan and black curves). The first one, at 8-14 pN with 2-3 nm extension change, was caused by folding of the partially closed syntaxin (Fig. 1D, state 6), while the second one, at 3-6 pN with 5-6 nm extension change, resulted from formation of the template complex of Munc18-1:syntaxin 1:VAMP2 (state 7) (37). All these observations are consistent with previous reports (11, 37, 39).

The addition of both 1 μM MUN domain and 1 μM Munc18-1 led to marked hysteresis in the unfolding and refolding of the template complex. In this case, the initial unfolding of the template complex during the pulling phase (Fig. 1C, #5-6, cyan arrows) occurred at significantly higher force than its initial refolding during the relaxation phase (#4-6, black arrows). We measured the unfolding and refolding forces and plotted their unimodal distributions (Fig. 1E) and cumulative distribution functions (SI Appendix, Fig. S2). The average unfolding and refolding forces were 8.5 ± 0.3 pN (mean ± SEM throughout the text, N=95) and 4.9 ± 0.1 pN (N=76), respectively. The difference between the unfolding force and the refolding force measured on the same pulling and relaxation cycle ranged from 1 pN to 9 pN (Fig. 1F). The large force hysteresis suggested a higher energy barrier for unfolding and refolding of the template complex in the presence of the MUN domain. In comparison, both transitions in the absence of the MUN domain reached thermal equilibrium at 5.1 ± 0.1 pN (the equilibrium force) without discernable hysteresis during pulling and relaxation (Fig. 1C, #2-3) (37). Thus, the MUN domain stabilized the template complex. However, MUN binding to the template complex barely change its extension relative to the unfolded syntaxin-VAMP conjugate (Fig. 1C, compare #4-6 to #2-3; Fig. 2), indicating that MUN binding likely did not significantly alter the conformation of the template complex. Consequently,

in our assay MUN binding was mainly inferred from the enhanced mechanical stability of the MUN-bound template complex. Finally, the MUN domain alone did not affect the unfolding of the ternary SNARE complex (Fig. 1C, compare the pulling FECs in #1 and #4), nor did it induce folding of the disordered syntaxin-VAMP conjugate (compare the relaxation FEC in #1 and the overlapping pulling and relaxation FECs in #7) under our experimental conditions. These observations are consistent with negligible associations of 1 μM MUN domain with individual syntaxin and VAMP2 molecules estimated from their large dissociation constants (> 40 μM) (19, 30, 31). In contrast, the MUN domain readily binds to and stabilizes the template complex (Fig. 1D, state 9).

Energetics and kinetics of MUN-bound template complex. To further characterize the MUN-bound template complex, we measured SNARE folding and unfolding transitions at constant mean force (42). We first compared the SNARE transitions at 5 pN in the presence of the MUN domain and/or Munc18-1 (Fig. 2). With the MUN domain alone, no SNARE folding was observed, consistent with the pulling result described above. In the presence of Munc18-1 alone, we detected fast transitions between the template complex and partially closed syntaxin, with an approximately equal probability of observing each state. With both Munc18-1 and the MUN domain, the template complex dominated (the third trace from the top), corroborating that the MUN domain stabilized the template complex. Higher force induced unfolding of the MUN-bound template complex. Once unfolded, the SNAREs generally failed to refold for an extended period time (up to 10 minutes) at constant mean force, confirming a large energy barrier to forming the MUN-bound template complex. Nevertheless, we observed a small number of trajectories with reversible template complex transitions that occurred at an average equilibrium force of 6.8 ± 0.1 pN (N=6; Fig. 2,

bottom trace). As expected, the transition was slow, with an equilibrium rate of 0.5 ± 0.3 s^{-1} revealed by hidden-Markov modeling (green trace), compared with an equilibrium rate of 3.2 ± 0.7 s^{-1} for the template complex in the absence of the MUN domain (37). Based on the mechanical work required to reversibly unfold the MUN-bound template complex (see Data analysis section in Materials and Methods), we estimated unfolding energy as 7.3 ± 0.4 k_BT for the MUN-bound template complex. Given the smaller unfolding energy 5.2 ± 0.2 k_BT of the template complex in the absence of the MUN domain (37), MUN domain binding significantly stabilizes the template complex.

MUN-bound template complex promotes SNAP-25B binding and SNARE assembly. We next tested whether the MUN-bound template complex supports SNAP-25B binding and SNARE assembly. To this end, we added 131 nM SNAP-25B, 1 μM Munc18-1, and 1 μM MUN domain in the solution. Under our experimental conditions, spontaneous SNARE assembly is inhibited by Munc18-1, as previously shown (37). To prepare the MUN-bound template complex, we first relaxed the unfolded syntaxin-VAMP conjugate to form the template complex (Fig. 3, #1, black arrow) and then pulled it to above 5 pN to confirm MUN domain binding (#2, cyan curve). Next, the MUN-bound template complex was held at a constant mean force to await SNAP-25B binding (#2, red region). Finally, the SNARE complex was relaxed and pulled again to reset to the unfolded state, after which we repeated the SNARE assembly cycle (#3-5). We found that SNAP-25B quickly associated with the MUN-bound template complex (Fig. 3B), as indicated by a single 8-9 nm extension drop (Figs. 3A & 3C, red arrows). The resultant SNARE complex exhibited the same extension and stepwise unfolding as the fully assembled SNARE complex (Fig. 3A, see the overlapping FECs in #1-3 and compare the gray FEC in #1 and cyan FECs in #3 and #5),

suggesting that SNAP-25B binding led to full SNARE assembly, likely by displacing the MUN domain and Munc18-1 from the four-helix bundle (Fig. 3B). In conclusion, the MUN-bound template complex supports SNARE assembly.

Next, we examined how the MUN domain and Munc18-1 may synergistically chaperone SNARE assembly. We initiated SNARE assembly by relaxing the unfolded syntaxin-VAMP conjugate in the presence of 1 μM Munc18-1 and 40 nM SNAP-25B and then holding it at 5 pN constant mean force, the force that permitted both MUN-dependent and MUN-independent SNARE assembly. After a maximum of 100 seconds, the conjugate was relaxed, pulled to confirm its folding status, and reset to the unfolded state. Finally, the procedure was repeated to detect the next round of SNARE assembly. The probability of SNARE assembly per round was scored and compared for the experiments in the absence and presence of 1 μM MUN domain. The addition of the MUN domain increased the SNARE assembly probability from 0.41 to 0.71 (Fig. 4). Thus, the MUN domain significantly promotes Munc18-1-chaperoned SNARE assembly.

To demonstrate the role of the MUN-bound template complex in chaperoned SNARE assembly, we repeated the above experiment but at a reduced Munc18-1 concentration of 0.25 μM. We found that the Munc18-1 concentration reduction decreased the probability of SNARE assembly in the absence of the MUN domain to 0.18, with no significant change in the SNARE assembly probability in the presence of the MUN domain (0.75). Taken together, our data confirm that the MUN domain and Munc18-1 cooperatively chaperone SNARE assembly via the MUN-bound template complex intermediate.

Conformation of the MUN-bound template complex and its potential physiological relevance. To further explore the MUN-bound template complex, we tested two modifications

that are reported to perturb MUN-SNARE interactions, SNARE assembly, and neurotransmitter release (25, 30, 31). The first modification is the introduction of two alanine substitutions, N1128A and F1131A (NFAA mutation), at the center of the MUN domain (Fig. 5, inset, & Fig. 1A) (25, 31). This modification impairs MUN domain binding to the N-terminal linker region of syntaxin 1 between the N-terminal regulatory domain (NRD) and the SNARE motif (Figs. 1B & 5). The second modification is truncation of the VAMP2 juxtamembrane linker domain (VAMP2 Δ85-96 or ΔLD) that was recently shown to bind one end of the MUN domain (Fig. 1A) (30). To quantify the effects of these modifications on the MUN-bound template complex, we repeatedly pulled and then relaxed the syntaxin-VAMP conjugate in the presence of 1 μM Munc18-1 and 1 μM MUN domain but in the absence of SNAP-25B. We found that both modifications dramatically decreased the probability of MUN binding to the template complex per relaxation (Fig. 5 & SI Appendix, Fig. S3). This observation suggests that both MUN-SNARE binding sites are crucial for the MUN domain to bind the template complex. Given the reported functional significance of these binding sites, our data imply that the MUN-bound template complex is indispensable for SNARE assembly and synaptic vesicle fusion in vivo.

Discussion

Electrophysiological measurements and imaging by electron and optical microscopy have demonstrated that synaptic vesicle fusion involves multiple intermediate states, including docking, priming, fusion pore opening and dilation (2, 43). How SNAREs and regulatory proteins mediate these states remains a central question in the field. Both Munc13-1 and Munc18-1 are involved in vesicle docking and priming, but the underlying molecular mechanism is unclear (1, 20, 21, 27, 44). It remains challenging to study interactions between SNAREs and their regulatory proteins,

partly because these interactions are generally weak and highly dynamic (19, 30-32). Using optical tweezers, we found that the MUN domain of Munc13-1, Munc18-1, syntaxin 1, and VAMP2 associate into a tetrameric complex to initiate SNARE assembly. Combined with previous studies, our finding implies that the complex may participate in vesicle docking and priming.

Our data also shed light on the structure of the tetrameric complex. Using single-molecule force spectroscopy, we recently identified the template complex consisting of Munc18-1, syntaxin, and VAMP2 that acts as an essential intermediate for Munc18-1-chaperoned SNARE assembly (37). In this template complex, Munc18-1 aligns the N-terminal regions of the SNARE motifs of syntaxin 1 and VAMP2 while keeping their C-terminal regions separated on the Munc18-1 surface. The NRD of syntaxin stabilizes the template complex. In contrast, the N-terminal linker region of syntaxin between the NRD and the SNARE motif and the C-terminal linker domain of VAMP2 do not appear to bind Munc18-1. Our data here show that the MUN domain binds both regions to stabilize the template complex and the MUN binding does not appear to significantly alter the extension of the template complex. The distance between the two regions inferred from the structural model of the template complex is consistent with the distance of the cognate binding sites on the MUN domain (Fig. 5, inset) (23, 25, 30, 37). Thus, the MUN domain binds both SNARE proteins at sites left accessible upon formation of the template complex and may stabilize the template complex by clamping the templated SNAREs in a half-zippered state. This binding mode exposes the SNARE motifs for SNAP-25 binding and subsequent SNARE assembly. The VAMP2 linker domain contains many positively charged and hydrophobic residues that are shown to strongly interact with membranes (45). Thus, the MUN domain may compete with the membrane to bind the linker domain of membrane-anchored VAMP2. In addition, trans-membrane binding of Munc13-1 via its terminal C1 and C2 domains (27) may affect its association with the

template complex. Synaptotagmin and complexin, as well as SNAP-25, may bind the tetrameric complex to form a partially-zippered SNARE complex to assist vesicle priming and resist premature SNARE disassembly by NSF/SNAP (4, 11, 14, 16, 37, 46). Finally, further calcium-triggered SNARE zippering complete membrane fusion, leading to displacement of regulatory proteins from the SNARE four-helix bundle.

It remains unclear how Munc13-1 opens Munc18-1-bound closed syntaxin to allow SNARE assembly. Although no clear intermediates have been observed in Munc13-1-catalyzed SNARE assembly starting from closed syntaxin (25, 30), it was hypothesized that Munc13-1 induces opening of the closed syntaxin upon binding to the binary complex (31, 37, 47). To test this hypothesis, we pulled single syntaxin along two directions in the presence of 1 μM Munc18-1 (48) and 1 μM MUN domain (SI Appendix, Fig. S4). We found that at this concentration, the MUN domain alone did not significantly affect the conformation of the closed syntaxin and its unfolding transition. Therefore, the MUN domain does not appear to directly induce opening of the closed syntaxin under our experimental conditions. We thus propose that Munc13-1 collaborates with VAMP2 to open closed syntaxin by forming the stabilized template complex. Consistent with this view, we found that the MUN-bound template complex is as stable as closed syntaxin (7.3 ± 0.4 k_BT vs 7.2 ± 0.2 k_BT) (37). Therefore, the template complex may thermodynamically compete with closed syntaxin to allow SNARE assembly. However, our data do not rule out the possibility that, at a higher concentration, the MUN domain binds the Munc18-1-syntaxin complex to slightly change the conformation of the closed syntaxin (31), because our assay is not sensitive to such minor conformational change (SI Appendix, Fig. S4).

In summary, the tetrameric complex identified by us may serve as a crucial intermediate to regulate SNARE assembly. Future work will examine how other regulatory proteins target the complex and cooperatively control synaptic vesicle fusion.

Materials and Methods

Protein constructs and purification. The cytoplasmic domains of rat syntaxin-1A (a.a. 1-265, R198C) and VAMP2 (a.a. 1-96, N29C), rat Munc18-1, and the MUN domain of rat Munc13-1 (a.a. 859-1407 and 1453-1531, with the loop region 1408-1452 replaced by EF residues) were described elsewhere in detail and were purified accordingly (19, 25, 30, 31, 37). Briefly, the MUN gene was cloned into the pGEX vector encoding a GST tag and a thrombin cleavage site N-terminal to the MUN sequence. The MUN protein was expressed in BL21 E. coli cells and purified using glutathione-agarose beads following by GST tag removal. Syntaxin 1A, VAMP2, and Munc18-1 genes were cloned into the pET-SUMO vector encoding six histidine followed by a SUMO tag at the N termini. The full-length rat SNAP-25B was cloned into pET-15b vector encoding six histidine tag at the N terminus. These SNAREs and Munc18-1 were expressed and purified from BL21 E. coli cells using Ni-NTA-agarose beads. Syntaxin-1A was biotinylated at its C terminal Avi-tag with the biotin ligase as previously described (49).

SNARE complex formation and crosslinking. Ternary SNARE complexes were prepared and crosslinked with DNA handles as was previously described (11, 37, 49). Briefly, ternary SNARE complexes were assembled by mixing the purified syntaxin-1A, SNAP-25B, and VAMP2 at molar ratio 0.8:1:1.2 and incubating at 4 °C overnight. Assembled SNARE complexes were purified by binding to Ni-NTA-agarose through the His-tag on SNAP-25B. The SNARE complexes were

crosslinked with DTDP (2,2'-dithiodipyridine disulfide) treated DNA handles with a molar ratio of 50:1 in 100 mM phosphate buffer, 500 mM NaCl, pH 8.5.

Single-molecule manipulation experiments. Dual-trap optical tweezers and basic protocols for single-molecule experiments have been described in detail elsewhere (40, 41). Briefly, the two optical traps were formed by focusing two orthogonally polarized beams by a water-immersed 60X objective with a 1.2 numerical aperture (Olympus, PA). The two beams were split from a single 1064 nm laser beam generated by a solid-state laser (Spectra-Physics, CA). One of the two beams is deflected by a mirror mounted on a piezoelectrically controlled stage that can tilt along two orthogonal axes (Mad City Labs, WI), which was used to move one trap relative to the other. The outgoing laser beams were collimated by a second water immersion objective, split, and projected onto two position-sensitive detectors (Pacific Silicon Sensor, CA). Bead displacements were detected by back-focal plane interferometry. Aliquots of the two DNA handles, one crosslinked with the SNARE complex and the other bound by a streptavidin molecule, were separately bound to anti-digoxigenin antibody coated polystyrene beads of 2.1 μm in diameter (Spherotech, IL). The two kinds of beads were injected into a microfluidic channel and trapped. The two beads are brought close to allow a single SNARE complex to be tethered between them. All manipulation experiments were carried out in PBS buffer supplemented with the oxygen scavenging system. All single molecules were pulled and relaxed by increasing and decreasing, respectively, the trap separation at a speed of 10 nm/sec or held at constant mean forces by keeping the trap separation constant (42).

Data analysis. Our methods were described in detail elsewhere (11, 42, 50). Briefly, the extension trajectories were analyzed by two-state hidden-Markov modeling (HMM), which yielded the probability, extension, force, and lifetime for each state (50). The unfolding energy of the MUN-bound template complex ΔG_u was determined based on the Boltzmann distribution under constant force, i.e., $\Delta G_u = F \times \Delta x - k_B T \times \ln K_u - \Delta G_s$, where F is the force, Δx is the extension increase associated with the equilibrium transition, K_u is the unfolding equilibrium constant, and ΔG_s is the entropic energy to stretch the unfolded syntaxin-VAMP conjugate to force F. At the equilibrium force $F_{1/2}$ with $K_u=1$ measured under our experimental conditions, $\Delta G_u = F_{1/2} \times \Delta x - \Delta G_s$, where the extension change Δx at the equilibrium force was determined based on the measured state extensions at constant trap separations, as is shown in Fig. S7 in ref. (11, 42). The entropic energy ΔG_s was calculated based on the worm-like chain model for the unfolded polypeptide, as is shown in Eq. 6 in ref. (11), with a persistence length of 0.6 nm and a contour length of 0.365 nm per amino acids.

Data availability. The MATLAB codes for our data analysis have been published elsewhere (11, 37).

Acknowledgements

We thank Josep Rizo for providing the plasmid for MUN domain purification and Fred Hughson for reading the manuscript. This work is supported by the NIH grants GM120193, GM131714, and GM093341 to Y. Z. and DK027044 to J. E. R.. T. S., Y. Z., and J. E. R. designed research; T. S., H. J., and Y. Z. performed research; T. S. analyzed data; T. S., Y. Z., and J. E. R. interpreted the results; T. S., Y. Z. and J. E. R. wrote the paper. The authors declare no interest of conflict.

References

1. T. C. Sudhof, J. E. Rothman, Membrane fusion: grappling with SNARE and SM proteins. *Science* **323**, 474-477 (2009).
2. P. S. Kaeser, W. G. Regehr, The readily releasable pool of synaptic vesicles. *Curr. Opin. Neurobiol.* **43**, 63-70 (2017).
3. A. T. Brunger, U. B. Choi, Y. Lai, J. Leitz, Q. J. Zhou, Molecular mechanisms of fast neurotransmitter release. *Ann Rev Biophys* **47**, 469-497 (2018).
4. R. W. Baker, F. M. Hughson, Chaperoning SNARE assembly and disassembly. *Nat Rev Mol Cell Biol* **17**, 465-479 (2016).
5. T. Sollner *et al.*, SNAP receptors implicated in vesicle targeting and fusion. *Nature* **362**, 318-324 (1993).
6. J. E. Rothman, The principle of membrane fusion in the cell (Nobel Lecture). *Angew Chem Int Edit* **53**, 12676-12694 (2014).
7. T. C. Sudhof, Neurotransmitter release: the last millisecond in the life of a synaptic vesicle. *Neuron* **80**, 675-690 (2013).
8. T. C. Sudhof, The molecular machinery of neurotransmitter release (Nobel lecture). *Angew Chem Int Edit* **53**, 12696-12717 (2014).
9. R. B. Sutton, D. Fasshauer, R. Jahn, A. T. Brunger, Crystal structure of a SNARE complex involved in synaptic exocytosis at 2.4 angstrom resolution. *Nature* **395**, 347-353 (1998).
10. P. I. Hanson, R. Roth, H. Morisaki, R. Jahn, J. E. Heuser, Structure and conformational changes in NSF and its membrane receptor complexes visualized by quick-freeze/deep-etch electron microscopy. *Cell* **90**, 523-535 (1997).
11. Y. Gao *et al.*, Single reconstituted neuronal SNARE complexes zipper in three distinct stages. *Science* **337**, 1340-1343 (2012).
12. J. Wang *et al.*, Calcium sensitive ring-like oligomers formed by synaptotagmin. *Proc. Natl. Acad. Sci. U.S.A.* **111**, 13966-13971 (2014).
13. M. J. Shon, H. Kim, T. Y. Yoon, Focused clamping of a single neuronal SNARE complex by complexin under high mechanical tension. *Nat Commun* **9** (2018).
14. Q. Zhou *et al.*, The primed SNARE-complexin-synaptotagmin complex for neuronal exocytosis. *Nature* **548**, 420-425 (2017).
15. M. Zhao *et al.*, Mechanistic insights into the recycling machine of the SNARE complex. *Nature* **518**, 61-67 (2015).
16. E. A. Prinslow, K. P. Stepien, Y. Z. Pan, J. Xu, J. Rizo, Multiple factors maintain assembled trans-SNARE complexes in the presence of NSF and alphaSNAP. *Elife* **8** (2019).
17. J. S. Shen, D. C. Tareste, F. Paumet, J. E. Rothman, T. J. Melia, Selective activation of cognate SNAREpins by Sec1/Munc18 proteins. *Cell* **128**, 183-195 (2007).
18. C. Ma, L. J. Su, A. B. Seven, Y. B. Xu, J. Rizo, Reconstitution of the vital functions of Munc18 and Munc13 in neurotransmitter release. *Science* **339**, 421-425 (2013).
19. Y. Lai *et al.*, Molecular mechanisms of synaptic vesicle priming by Munc13 and Munc18. *Neuron* **95**, 591-607 (2017).
20. I. Augustin, C. Rosenmund, T. C. Sudhof, N. Brose, Munc13-1 is essential for fusion competence of glutamatergic synoptic vesicles. *Nature* **400**, 457-461 (1999).

21. B. Aravamudan, T. Fergestad, W. S. Davis, C. K. Rodesch, K. Broadie, Drosophila Unc-13 is essential for synaptic transmission. *Nat. Neurosci.* **2**, 965-971 (1999).
22. S. Brenner, Genetics of Caenorhabditis-Elegans. *Genetics* **77**, 71-94 (1974).
23. J. J. Xu *et al.*, Mechanistic insights into neurotransmitter release and presynaptic plasticity from the crystal structure of Munc13-1 C1C2BMUN. *Elife* **6** (2017).
24. J. Basu *et al.*, A minimal domain responsible for Munc13 activity. *Nat. Struct. Mol. Biol.* **12**, 1017-1018 (2005).
25. X. Y. Yang *et al.*, Syntaxin opening by the MUN domain underlies the function of Munc13 in synaptic-vesicle priming. *Nat. Struct. Mol. Biol.* **22**, 547-754 (2015).
26. X. X. Liu *et al.*, Functional synergy between the Munc13 C-terminal C-1 and C-2 domains. *Elife* **5** (2016).
27. B. Quade *et al.*, Membrane bridging by Munc13-1 is crucial for neurotransmitter release. *Elife* **8** (2019).
28. F. Michelassi, H. W. Liu, Z. T. Hu, J. S. Dittman, A C1-C2 module in Munc13 inhibits calcium-dependent neurotransmitter release. *Neuron* **95**, 577-590 (2017).
29. O. H. Shin *et al.*, Munc13 C2B domain is an activity-dependent Ca2+ regulator of synaptic exocytosis. *Nat. Struct. Mol. Biol.* **17**, 280-U242 (2010).
30. S. Wang *et al.*, Munc18 and Munc13 serve as a functional template to orchestrate neuronal SNARE complex assembly. *Nat Commun* **10** (2019).
31. S. Wang *et al.*, Conformational change of syntaxin linker region induced by Munc13s initiates SNARE complex formation in synaptic exocytosis. *EMBO J.* **36**, 816-829 (2017).
32. C. Ma, W. Li, Y. Xu, J. Rizo, Munc13 mediates the transition from the closed syntaxin-Munc18 complex to the SNARE complex. *Nat Struct Mol Biol* **18**, 542-549 (2011).
33. K. M. S. Misura, R. H. Scheller, W. I. Weis, Three-dimensional structure of the neuronal-Sec1-syntaxin 1a complex. *Nature* **404**, 355-362 (2000).
34. P. Burkhardt, D. A. Hattendorf, W. I. Weis, D. Fasshauer, Munc18a controls SNARE assembly through its interaction with the syntaxin N-peptide. *EMBO J.* **27**, 923-933 (2008).
35. I. Dulubova *et al.*, A conformational switch in syntaxin during exocytosis: role of munc18. *EMBO J.* **18**, 4372-4382 (1999).
36. J. Pevsner *et al.*, Specificity and Regulation of a Synaptic Vesicle Docking Complex. *Neuron* **13**, 353-361 (1994).
37. J. Jiao *et al.*, Munc18-1 catalyzes neuronal SNARE assembly by templating SNARE association. *Elife* **7**, e41771 (2018).
38. R. W. Baker *et al.*, A direct role for the Sec1/Munc18-family protein Vps33 as a template for SNARE assembly. *Science* **349**, 1111-1114 (2015).
39. Y. L. Zhang, Energetics, kinetics, and pathway of SNARE folding and assembly revealed by optical tweezers. *Protein Sci.* **26**, 1252-1265 (2017).
40. G. Sirinakis, Y. X. Ren, Y. Gao, Z. Q. Xi, Y. L. Zhang, Combined and versatile high-resolution optical tweezers and single-molecule fluorescence microscopy. *Rev Sci Instrum* **83**, 093708 (2012).
41. J. R. Moffitt, Y. R. Chemla, D. Izhaky, C. Bustamante, Differential detection of dual traps improves the spatial resolution of optical tweezers. *Proc. Natl. Acad. Sci. U.S.A.* **103**, 9006-9011 (2006).

42. A. A. Rebane, L. Ma, Y. L. Zhang, Structure-based derivation of protein folding intermediates and energies from optical tweezers. *Biophys J* **110**, 441-454 (2016).
43. W. Shin *et al.*, Visualization of membrane pore in live cells reveals a dynamic-pore theory governing fusion and endocytosis. *Cell* **173**, 934-945 e912 (2018).
44. J. E. Rothman, S. S. Krishnakumar, K. Grushin, F. Pincet, Hypothesis - buttressed rings assemble, clamp, and release SNAREpins for synaptic transmission. *FEBS Lett* **591**, 3459-3480 (2017).
45. K. D. Brewer, W. Li, B. E. Horne, J. Rizo, Reluctance to membrane binding enables accessibility of the synaptobrevin SNARE motif for SNARE complex formation. *Proc. Natl. Acad. Sci. U.S.A.* **108**, 12723-12728 (2011).
46. E. Q. He *et al.*, Munc13-1 and Munc18-1 together prevent NSF-dependent de-priming of synaptic vesicles. *Nat Commun* **8**, 15915 (2017).
47. J. E. Richmond, R. M. Weimer, E. M. Jorgensen, An open form of syntaxin bypasses the requirement for UNC-13 in vesicle priming. *Nature* **412**, 338-341 (2001).
48. L. Ma *et al.*, Munc18-1-regulated stage-wise SNARE assembly underlying synaptic exocytosis. *eLIFE* **4**, e09580 (2015).
49. J. Y. Jiao, A. A. Rebane, L. Ma, Y. L. Zhang, Single-molecule protein folding experiments using high-resolution optical tweezers. *Methods Mol Biol* **1486**, 357-390 (2017).
50. Y. L. Zhang, J. Jiao, A. A. Rebane, Hidden Markov modeling with detailed balance and its application to single protein folding *Biophys J* **111**, 2110-2124 (2016).

Figure legends

Fig. 1. Optical tweezers reveal a template complex stabilized by the MUN domain. (A) Different functional domains of Munc13-1 with their boarders labeled by a.a. numbers. Amino acids in two distinct SNARE binding sites (N1128/F1131 and D1358) are indicated. (B) Schematic diagram of the experimental setup. A single SNARE complex (PDB ID 1SFC) was pulled from the C-termini of syntaxin 1A (red) and VAMP2 (blue) via two DNA handles attached to two optically trapped beads. The N-termini of both SNARE proteins were crosslinked via a disulfide bond. Munc18-1 (gray, derived from PDB ID 3C98) and the MUN domain of Munc13-1 (yellow, PDB ID 5UE8) were added in the solution. The syntaxin 1A molecule contains the N-terminal regulatory domain (NRD). (C) Representative force-extension curves (FECs) obtained in the presence (+) or absence (-) of 1 μM MUN domain or 1 μM Munc18-1. The syntaxin-VAMP

conjugate was pulled or relaxed by changing the separation between two optical traps at a speed of 10 nm/sec. Throughout the figures, all FECs are color coded in the same fashion: gray for pulling the initial purified SNARE complex, cyan for subsequent pulls, and black for relaxations. FECs obtained from consecutive pulling/relaxation rounds (e.g., #4-6) are offset along the x-axis and indicated by the same lines above the FECs. States associated with different FEC regions (indicated by red dashed lines if necessary) are indicated by the corresponding state numbers (see D; SI Appendix, Fig. S1; and Video 1 in ref. (37)). (D) Schematic diagrams of different SNARE folding and protein binding states: 4, fully unfolded SNARE motifs; 5, unfolded SNARE motifs with Munc18-1 bound; 6, partially closed syntaxin; 7, template complex; 8, assembled SNARE complex; and 9, MUN-bound template complex (11, 37). Other states are depicted in SI Appendix, Fig. S1. (E) Histogram distributions of the unfolding and refolding forces of all MUN-bound template complexes. The corresponding cumulative distribution functions are shown in SI Appendix, Fig. S2. (F) Histogram distribution of the difference between the unfolding force and the refolding of the MUN-bound template complexes.

Fig. 2. Extension-time trajectories at indicated constant mean forces in the absence or presence of 1 μM Munc18-1 or 1 μM MUN domain. The equilibrium force in the presence of the MUN domain (~6.8 pN) is higher than that in its absence (~5 pN), indicating that the MUN domain stabilizes the template complex. The red dashed lines indicate the average extensions of the indicated states (Figs. 1D & S1). The trajectories were obtained at constant trap separations, with the corresponding mean forces calculated as the means of two state forces (42).

Fig. 3. Mun-bound template complex supports efficient SNAP-25B binding and SNARE assembly. (A) FECs obtained by consecutively pulling and relaxing a single syntaxin-VAMP conjugate for five rounds in the presence of MUN, Munc18-1, and SNAP-25B with their concentrations indicated. During relaxation, the SNAREs were held at constant mean forces to allow SNAP-25B biding (red regions). The corresponding time-dependent extension trajectories are shown in C. Binding by the MUN domain and SNAP-25B are indicated by black arrows and red arrows, respectively. (B) Schematic diagram of SNARE assembly mediated by the MUN-bound template complex. (C) Extension-time trajectories at indicated constant mean forces showing SNAP-25B binding to the MUN-bound template complex. The red dashed lines indicate the average extensions of the corresponding states labeled with their state numbers in red (Fig. 1D).

Fig. 4. Probability of chaperoned SNARE assembly observed within 100 seconds at 5 pN constant mean force in the presence of 40 nM SNAP-25B and different concentrations of Munc18-1 and the MUN domain. The N value refers to the total number of trials for SNAP-25B binding as described in the text, and the error bar indicates the standard error of the mean.

Fig. 5. Probability of MUN binding to the template complex observed per round of pulling and relaxation for the WT and altered MUN domain or VAMP2. The inset shows a structural model of the MUN-bound template complex and the two modifications tested. The probability of MUN binding was calculated as the ratio of the total occurrence number of MUN-stabilized template complexes to that of all template complexes measured in all pulling rounds. The N value refers to the total round of pulling and relaxation, and the error bar indicates the standard error of the mean.

Fig. S1. Schematic diagrams of different states: 1, fully assembled SNARE complex; 2, half-zippered SNARE bundle; 3, t-SNARE complex; 4, fully unfolded SNARE motifs; 5, unfolded SNARE motifs with Munc18-1 bound to the NRD; 6, partially closed syntaxin; 7, template complex; 8, assembled SNARE complex with Munc18-1 bound to the NRD; and 9, MUN-bound template complex. These states and their transitions were derived from this study, as well as previous studies (11, 37).

Fig. S2. Cumulative distribution functions of the unfolding and refolding forces of the MUN-bound template complex, which correspond to the histogram distributions shown in Fig. 1E-F.

Fig. S3. Force-extension curves showing MUN-bound template complexes containing VAMP2 ΔLD (A) or MUN mutation NFAA (B). Assembly and disassembly of the MUN-bound template complex are indicated by black arrows and cyan arrows, respectively. The occurrence probabilities of both mutant MUN-bound template complexes per round of pulling and relaxation are reduced compared to the WT (Fig. 5).

Fig. S4. MUN domain does not directly open closed syntaxin under our experimental conditions, as is indicated by the minimum effect of 1 μM MUN domain on the syntaxin transition. (A) Schematic diagram to pull the SNARE motif of a single syntaxin 1A molecule (syntaxin 1A 1-265, I187C) at its C-terminus and I187C (37). Note that the mutation I187C does not significantly perturb the fully closed syntaxin conformation (state 6'), as is indicated by its crystal structure (33). (B) FECs obtained in the presence of 1 μM Munc18-1 alone or together with 1 μM MUN domain

in the solution. (C) Schematic diagram to pull a single syntaxin 1A molecule (syntaxin 1A 1-265, with a cysteine residue inserted after D25) from its C-terminus and N-terminus at D25 (48). (D) FECs obtained by pulling single syntaxin 1A molecules as shown in C in the presence or absence of 1 μM Munc18-1 (48) or 1 μM MUN domain. The inset shows the structural models of different syntaxin 1A folding and Munc18-1 binding states involved in the pulling experiment: closed Munc18-1-bound syntaxin (state i), open syntaxin with or without bound Munc18-1 (ii), and completely unfolded syntaxin (iii). Transitions between these states are indicated by arrows. Habc represents the antiparallel three-helix bundle in the N-terminal regulatory domain (NRD) of syntaxin. The MUN domain barely changed the average unfolding and refolding forces of the closed syntaxin. Consistent results from the two syntaxin pulling experiments imply that the pulling sites do not affect MUN binding, if there is any.

Figure 1

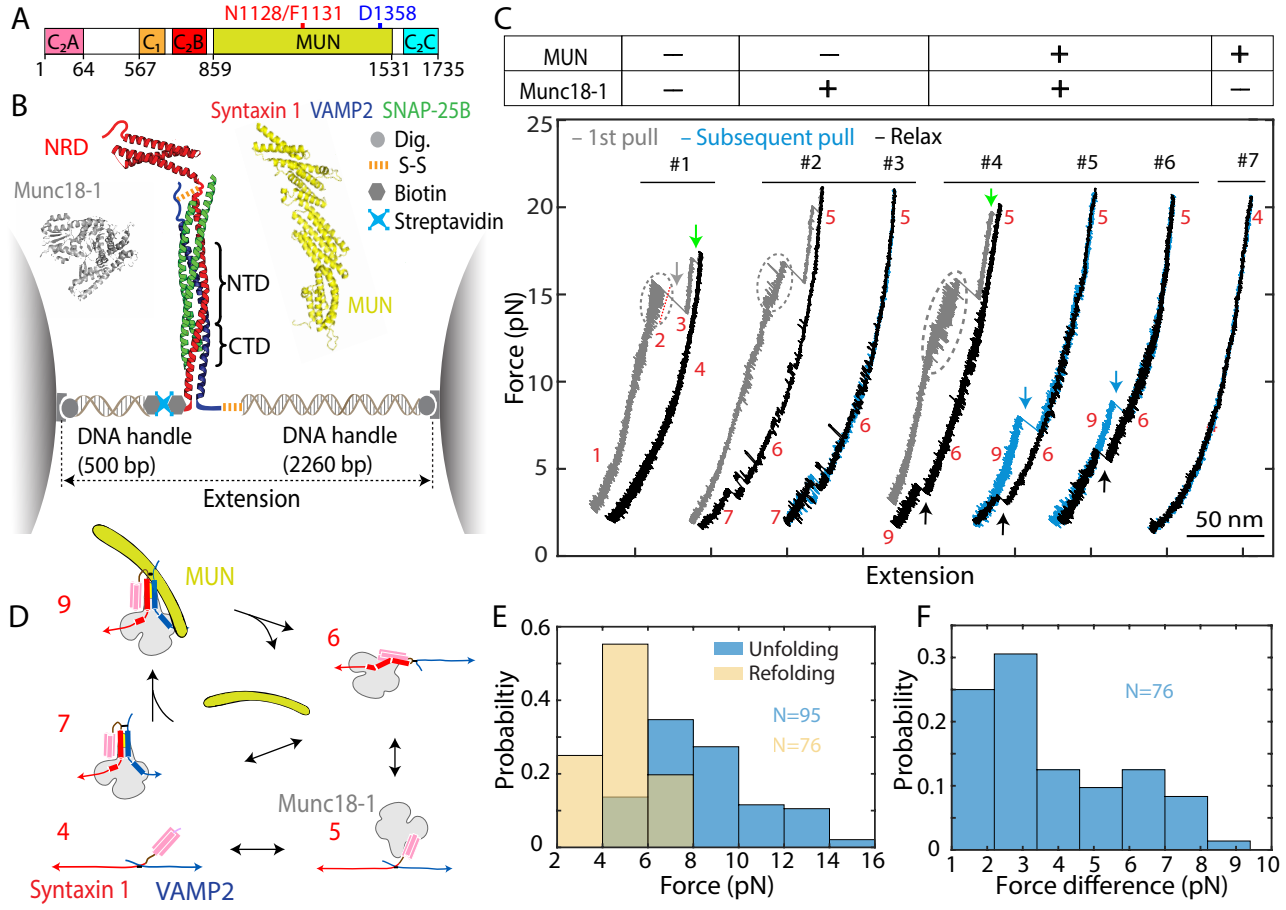
A
N1128/F1131
D1358
C2A
C1
C2B
MUN
C2C
1
64
567
859
1531
1735
B
Syntaxin 1
VAMP2
SNAP-25B
NRD
Munc18-1
Dig.
S-S
Biotin
Streptavidin
NTD
CTD
MUN
DNA handle
(500 bp)
DNA handle
(2260 bp)
Extension
C
MUN
Munc18-1
– 1st pull
– Subsequent pull
– Relax
#1
#2
#3
#4
#5
#6
#7
Force (pN)
Extension
50 nm
D
MUN
Munc18-1
Syntaxin 1
VAMP2
E
Unfolding
Refolding
N=95
N=76
Probability
Force (pN)
F
N=76
Probability
Force difference (pN)

Figure 2

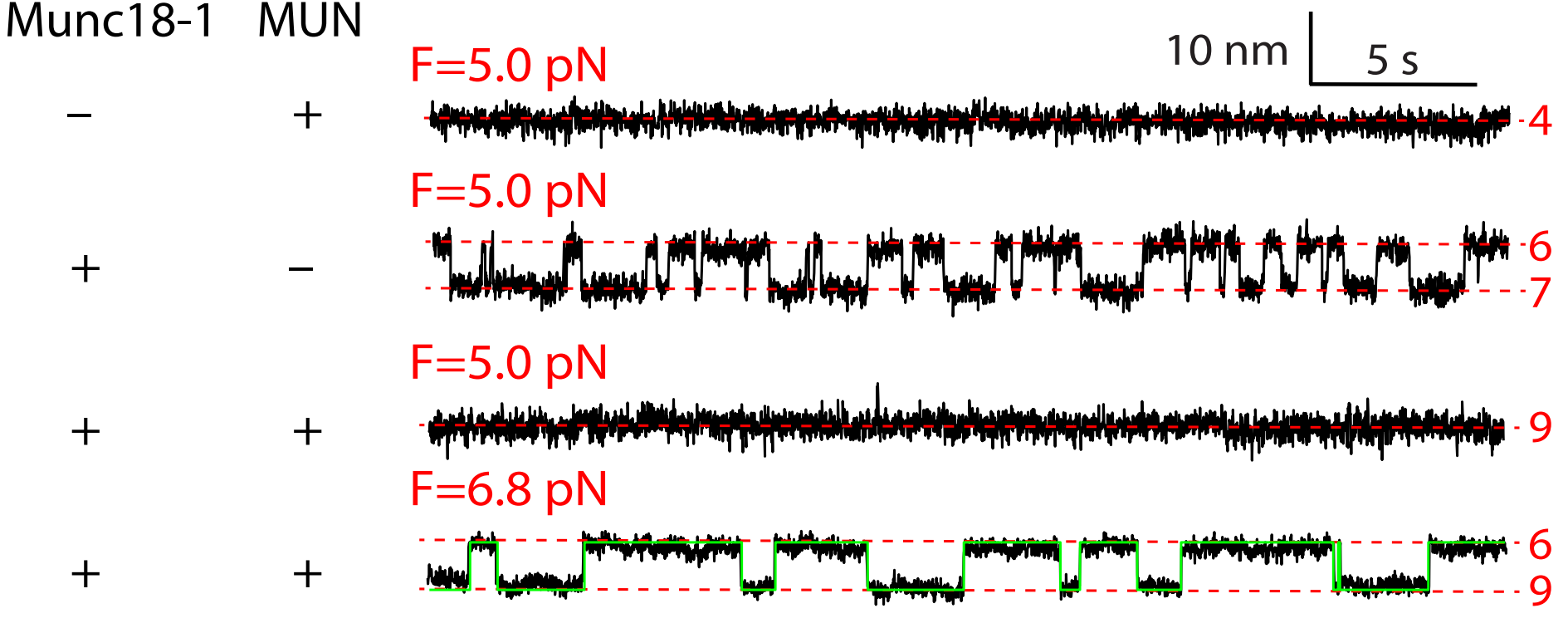

Figure 3

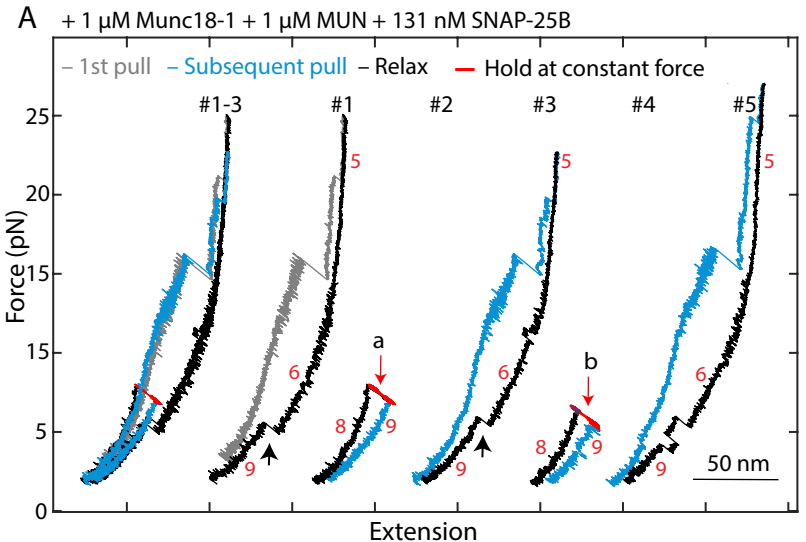
A
+ 1 µM Munc18-1 + 1 µM MUN + 131 nM SNAP-25B
– 1st pull
– Subsequent pull
– Relax
Hold at constant force
#1-3
#1
#2
#3
#4
#5
Force (pN)
Extension
50 nm
a
b

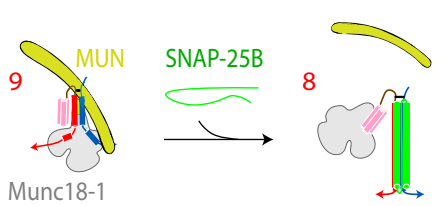
B
MUN
SNAP-25B
Munc18-1

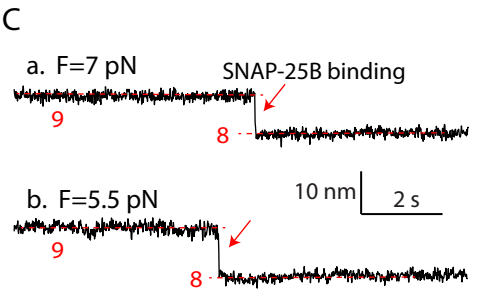
C
a. F=7 pN
SNAP-25B binding
b. F=5.5 pN
10 nm
2 s

Figure 4

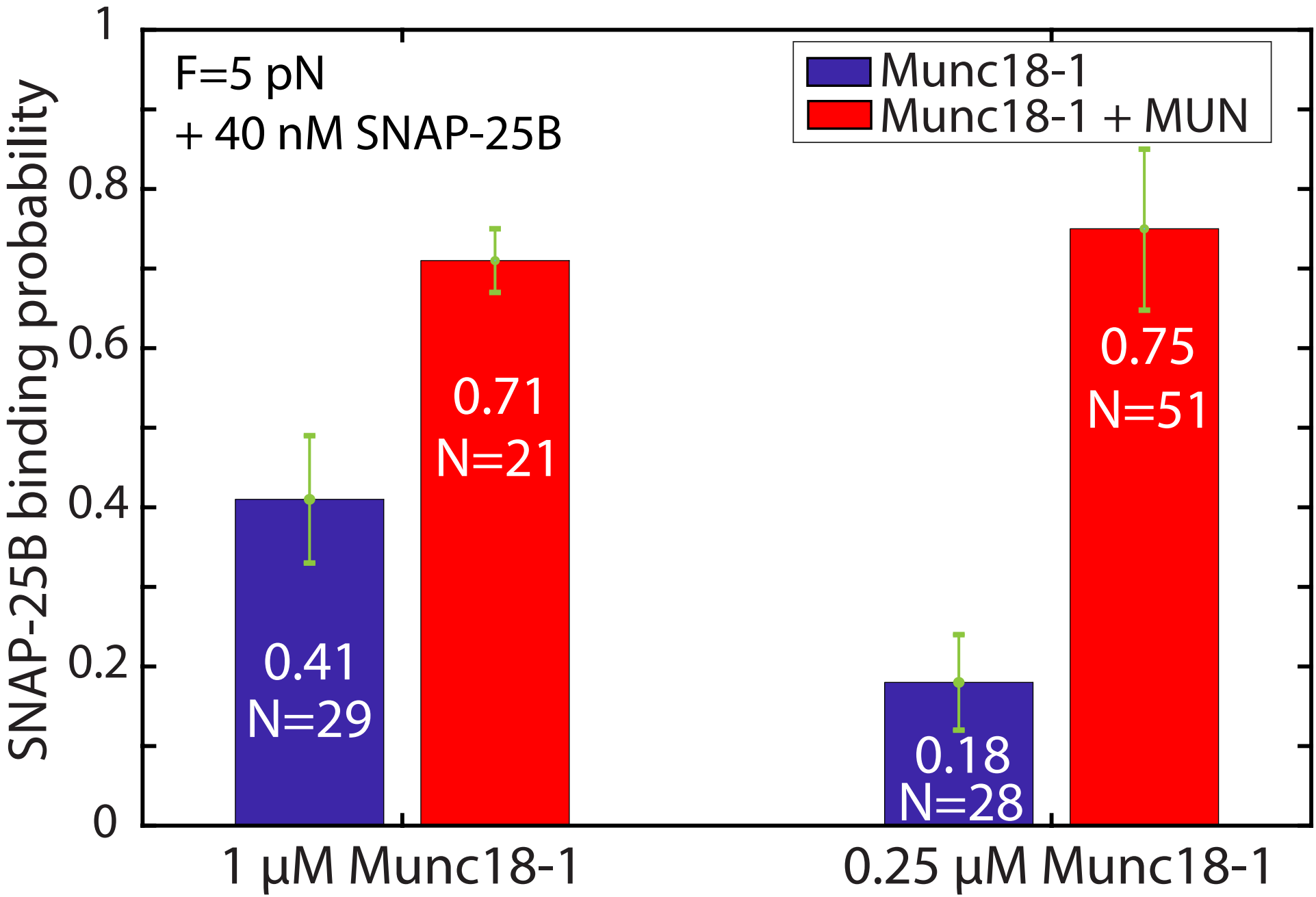
F=5 pN
+ 40 nM SNAP-25B
Munc18-1
Munc18-1 + MUN
SNAP-25B binding probability
1
0.8
0.6
0.4
0.2
0
0.41
N=29
0.71
N=21
0.18
N=28
0.75
N=51
1 μM Munc18-1
0.25 μM Munc18-1

Figure 5

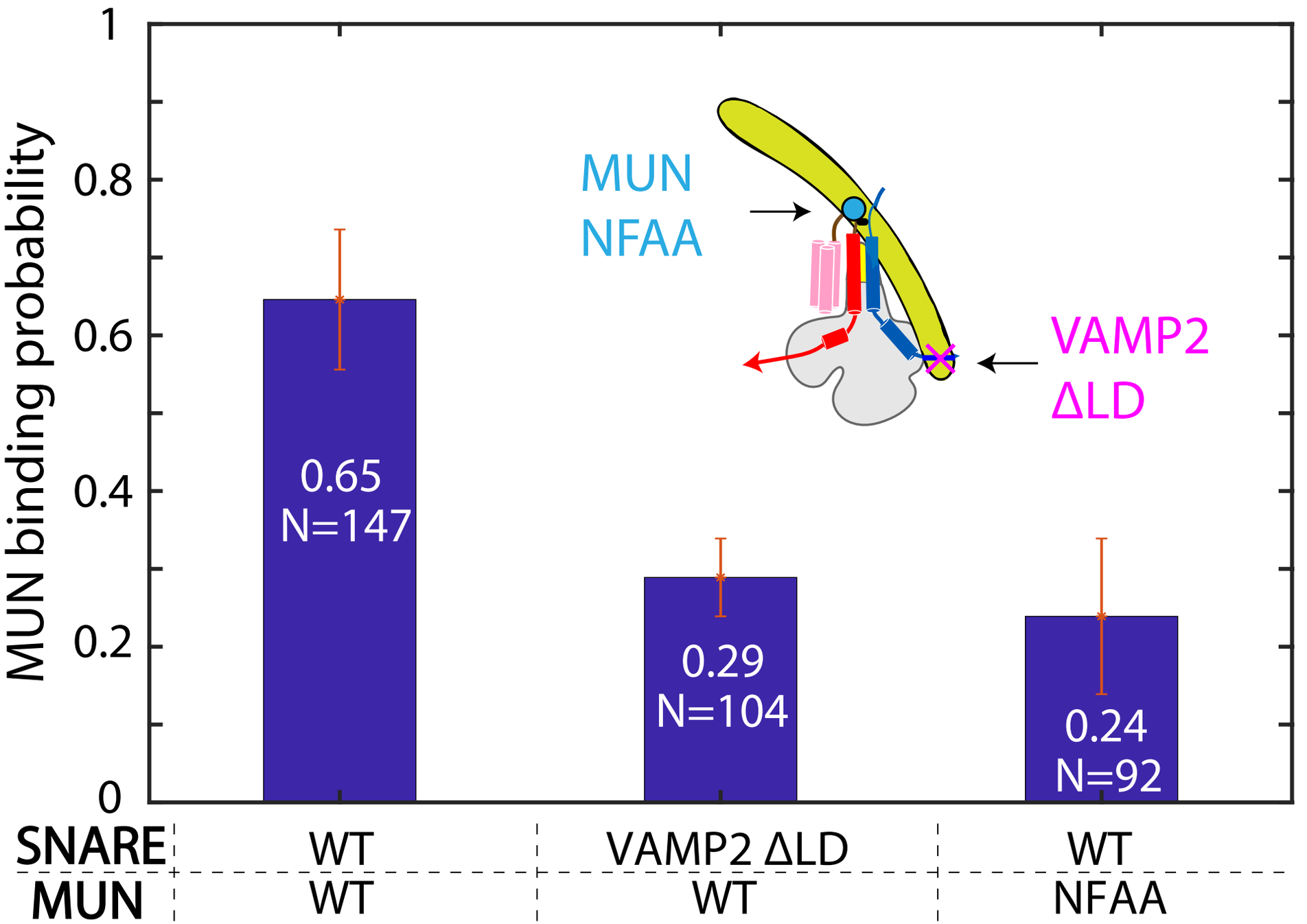
MUN binding probability
1
0.8
0.6
0.4
0.2
0
0.65
N=147
0.29
N=104
0.24
N=92
MUN
NFAA
VAMP2
ΔLD
SNARE
WT
VAMP2 ΔLD
WT
MUN
WT
WT
NFAA

Supplementary Information for

Munc13-1 MUN domain and Munc18-1 cooperatively chaperone SNARE assembly through a tetrameric complex

Tong Shu[a,b,c], Huaizhou Jin[a], James E. Rothman[a,1], and Yongli Zhang[a,1]

[a]Department of Cell Biology, Yale University School of Medicine, New Haven, CT 06520

[b]Integrated Graduate Program in Physical and Engineering Biology,

[c]Department of Physics, Yale University, New Haven, CT 06511.

[1]To whom correspondence may be addressed:
Yongli Zhang
Email: yongli.zhang@yale.edu
James E. Rothman
Email: james.rothman@yale.edu

This PDF file includes:

Figs. S1 to S4
References for SI reference citations

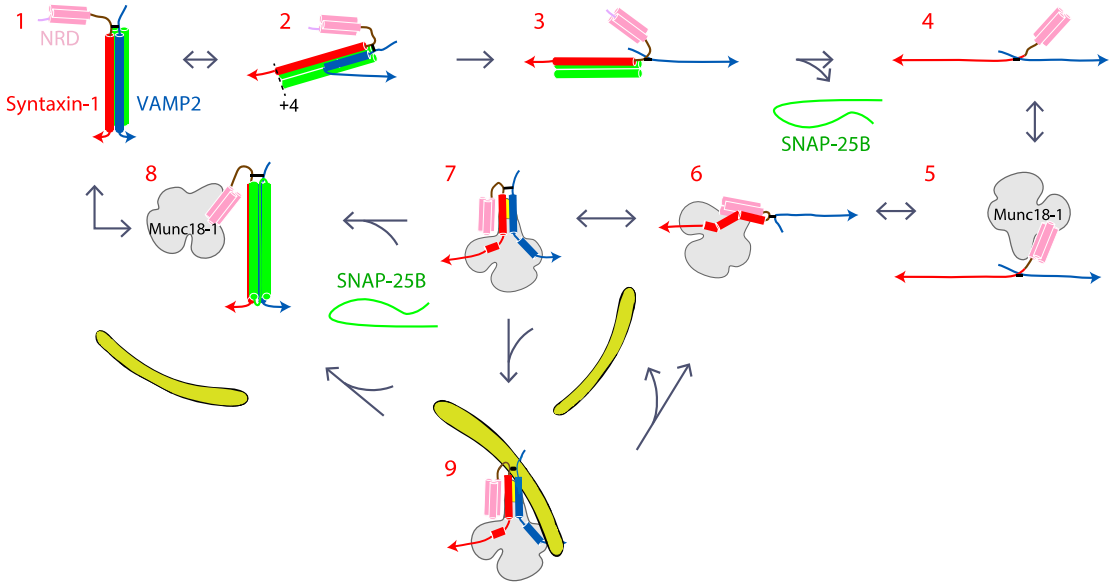

Fig. S1. Schematic diagrams of different states: 1, fully assembled SNARE complex; 2, half-zippered SNARE bundle; 3, t-SNARE complex; 4, fully unfolded SNARE motifs; 5, unfolded SNARE motifs with Munc18-1 bound to the NRD; 6, partially closed syntaxin; 7, template complex; 8, assembled SNARE complex with Munc18-1 bound to the NRD; and 9, MUN-bound template complex. These states and their transitions were derived from this study, as well as previous studies (1, 2).

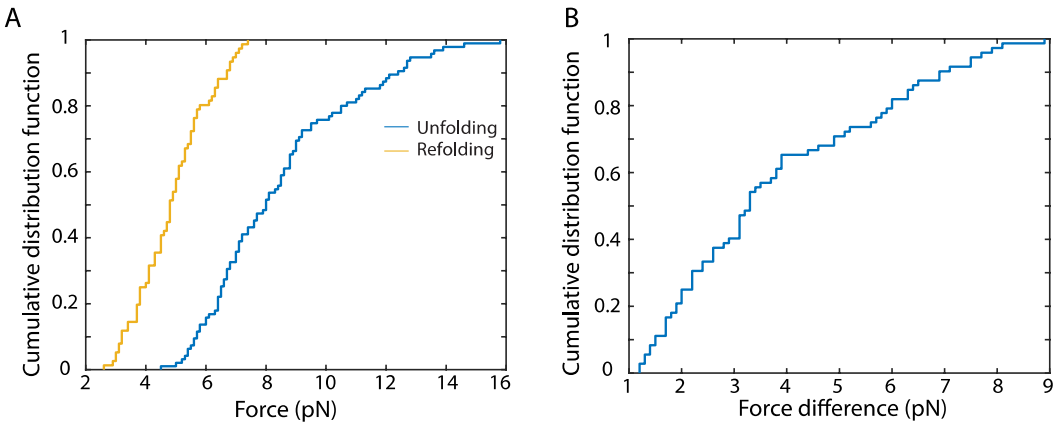

Fig. S2. Cumulative distribution functions of the unfolding and refolding forces of the MUN-bound template complex, which correspond to the histogram distributions shown in Fig. 1E-F.

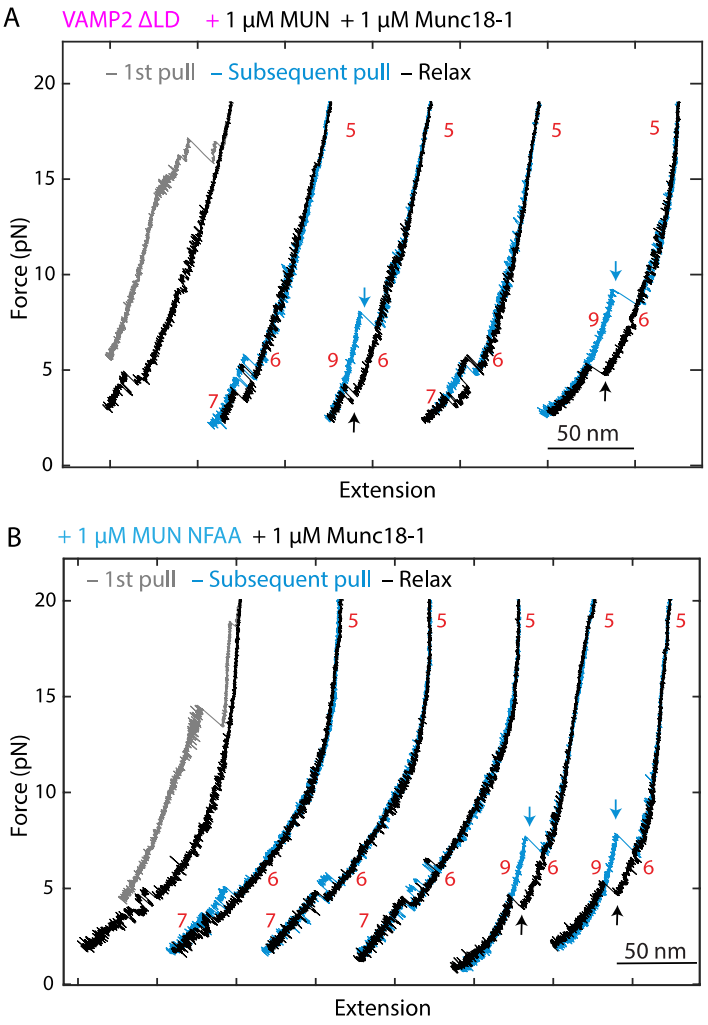

Fig. S3. Force-extension curves showing MUN-bound template complexes containing VAMP2 ΔLD (A) or MUN mutation NFAA (B). Assembly and disassembly of the MUN-bound template complex are indicated by black arrows and cyan arrows, respectively. The occurrence probabilities of both mutant MUN-bound template complexes per round of pulling and relaxation are reduced compared to the WT (Fig. 5).

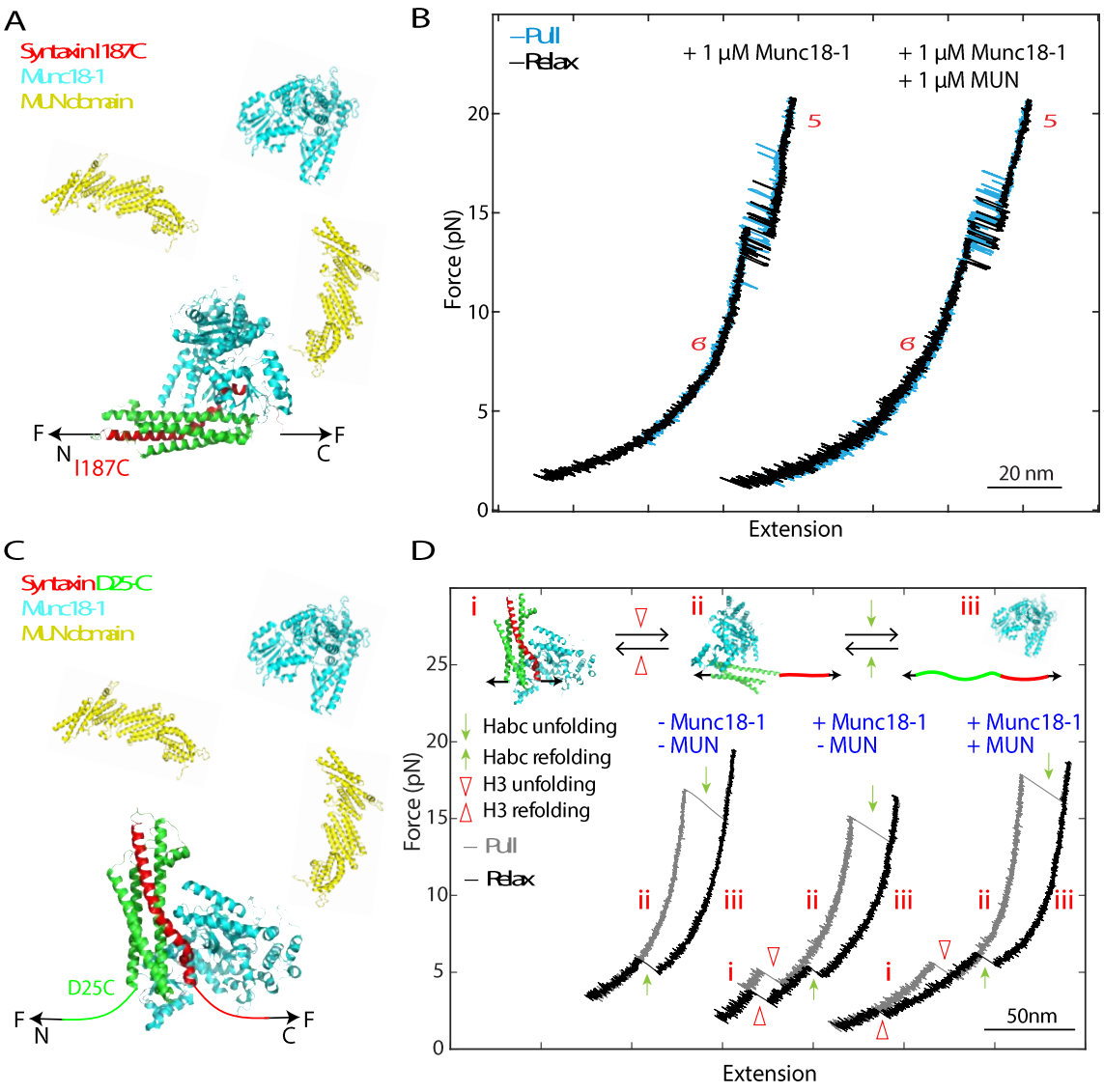

Fig. S4. MUN domain does not directly open closed syntaxin under our experimental conditions, as is indicated by the minimum effect of 1 μM MUN domain on the syntaxin transition. (A) Schematic diagram to pull the SNARE motif of a single syntaxin 1A molecule (syntaxin 1A 1-265, I187C) at its C-terminus and I187C (2). Note that the mutation I187C does not significantly perturb the fully closed syntaxin conformation (state 6'), as is indicated by its crystal structure (3). (B) FECs obtained in the presence of 1 μM Munc18-1 alone or together with 1 μM MUN domain in the solution. (C) Schematic diagram to pull a single syntaxin 1A molecule (syntaxin 1A 1-265, with a cysteine residue inserted after D25) from its C-terminus and N-terminus at D25 (4). (D) FECs obtained by pulling single syntaxin 1A molecules as shown in C in the presence or absence of 1 μM Munc18-1 (4) or 1 μM MUN domain. The inset shows the structural models of different

syntaxin 1A folding and Munc18-1 binding states involved in the pulling experiment: closed Munc18-1-bound syntaxin (state i), open syntaxin with or without bound Munc18-1 (ii), and completely unfolded syntaxin (iii). Transitions between these states are indicated by arrows. Habc represents the antiparallel three-helix bundle in the N-terminal regulatory domain (NRD) of syntaxin. The MUN domain barely changed the average unfolding and refolding forces of the closed syntaxin. Consistent results from the two syntaxin pulling experiments imply that the pulling sites do not affect MUN binding, if there is any.

References

1. Y. Gao *et al.*, Single reconstituted neuronal SNARE complexes zipper in three distinct stages. *Science* **337**, 1340-1343 (2012).
2. J. Jiao *et al.*, Munc18-1 catalyzes neuronal SNARE assembly by templating SNARE association. *Elife* **7** (2018).
3. K. M. Misura, R. H. Scheller, W. I. Weis, Three-dimensional structure of the neuronal-Sec1-syntaxin 1a complex. *Nature* **404**, 355-362 (2000).
4. L. Ma *et al.*, Munc18-1-regulated stage-wise SNARE assembly underlying synaptic exocytosis. *Elife* **4** (2015).